Study of Subcooled Film Boiling on a Horizontal Disc:[1] Part 2—Experiments

D. Banerjee

V. K. Dhir

Mechanical and Aerospace Engineering Department, University of California, Los Angeles, Los Angeles, CA 90095

Experiments were performed to study subcooled film boiling of performance liquid PF-5060 (made by 3-M Company) on a horizontal copper disc. The experiments were performed for two regimes of film boiling involving departing vapor bubbles (low subcooling) and nondeparting vapor bubbles (high subcooling). By employing high speed digital camera, data were obtained for temporal variation of bubble height, bubble shape and bubble growth rate over one cycle. Heat flux data were deduced from temperatures measured with thermocouples embedded in the solid. The results from the numerical model are compared with experimental data and are found to be in general agreement. Particle Tracking Velocimetry (PTV) experiments were performed for a configuration of non-departing vapor bubbles to study the flow field in the liquid phase. The PTV experiments point to the existence of natural convection flow in the liquid phase and is in qualitative agreement with the predictions available in the literature.
[DOI: 10.1115/1.1345890]

Keywords: Boiling, Film, Heat Transfer, Phase Change, Two-Phase

1 Introduction

In subcooled film boiling the bulk temperature of the liquid phase is lower than the saturation temperature. In such a situation the heat flux at the wall is partitioned at the interface between phase change and convective heat transfer into the subcooled liquid. This results in higher heat transfer compared to saturated film boiling.

Dhir and Purohit [1] observed experimentally that film boiling heat transfer coefficients in subcooled film boiling on a sphere were 50–60 percent higher than those predicted by the laminar plane interface theory. The significant enhancement in liquid side heat transfer was attributed to the alteration of flow field in the liquid by interfacial waves. Experimental results of Vijaykumar and Dhir [2,3] show that degree of subcooling significantly affects the liquid side heat transfer in subcooled film boiling on a flat vertical plate.

Nishio and Ohtake [4] observed that subcooled film boiling in the ''small cylinder diameter'' regime could be divided into two distinct regimes, ''normal'' and ''singular.'' In the ''normal'' regime of film boiling (for R-113 as the test fluid and for heater wire diameter greater than 0.2 mm) the boiling heat transfer coefficient was found to increase with degree of subcooling. In the ''singular'' regime of film boiling (for R-113 as the test fluid and heater wire diameter less than 0.2 mm), the heat transfer coefficients were found to decrease to a minimum with increasing subcooling. However, the authors did not provide any explanation for this peculiar behavior in the ''singular'' regime.

Kikuchi et al. [5] found that in saturated film boiling of water on silver coated spherical and cylindrical probes the liquid-solid (L-S) contacts occurred with a much higher frequency compared to subcooled film boiling, in which the L-S contacts were almost nonexistent. This pointed to the stabilizing influence of subcooling on the vapor-liquid interface in subcooled film boiling. They also found that the L-S contact frequency was lower for a cylinder than for a sphere.

Linear stability analysis performed by Busse and Schubert [6] and also discussed by Busse [7], for a system undergoing first order phase change by heating from below pointed to the existence of different regimes of vapor-liquid interfacial instability. An application of this analysis was in a geothermal situation where, for instance, water can be stably stratified over steam. The results of the aforementioned analysis were experimentally verified by Ahlers et al. [8]. The experiments involved isotropic-nematic phase transition of a liquid crystal. They reported various conditions where conduction temperature profile was obtained in the heavier overlying nematic phase.

Under certain conditions of subcooling and wall heat flux values the vapor film is stably stratified under the liquid pool in subcooled film boiling under pool boiling conditions. Study of such a configuration is helpful in understanding the hydrodynamic aspects of the vapor-liquid interface and heat transfer into the subcooled liquid. Such a situation was reported by Ayazi and Dhir [9], for subcooled film boiling of water on a horizontal cylinder. The authors argued that such a configuration of stationary vapor-liquid interface can exist only when the vapor production rate at the film matches the condensation rate at the bubble interface. Based on the experimental results, the authors proposed a criterion for the onset of collapse of subcooled film boiling on a horizontal cylinder.

Though there is a huge body of literature on subcooled film boiling—very few investigations have been performed to understand the hydrodynamics of film boiling on a horizontal flat plate. Part of the reason can be ascribed to the difficulty in gathering experimental data for evolution of the interface on a flat plate (compared to say, on a horizontal cylinder) and also in proper post processing of the experimental data. The difficulty arises because of obstruction of the view by bubbles departing in front and back of the focal plane. This study was performed to enhance the understanding of subcooled film boiling on a horizontal flat plate under pool boiling conditions. The objectives of the present investigation were to: (1) compare the hydrodynamic and wall heat transfer experimental data with numerical predictions for a configuration of departing bubbles at low subcoolings; and (2) study the occurrence of a stably stratified vapor layer under the liquid pool for subcooled film boiling on a horizontal disc at high subcoolings and compare the results with the numerical predictions of Banerjee et al. [10].

For this purpose, film boiling experiments were performed from low to high subcoolings. In the experiments, spacing of the bubble

[1]This work received support from the National Science Foundation.

Contributed by the Heat Transfer Division for publication in the JOURNAL OF HEAT TRANSFER. Manuscript received by the Heat Transfer Division January 20, 2000; revision received October 31, 2000. Associate Editor: V. Carey.

releasing nodes, bubble shape during the evolution of the interface, bubble growth rate, flow field in the liquid and overall heat transfer rate were measured.

2 Experimental Apparatus

The experimental setup is shown in Fig. 1. The test section consists of a cylindrical test heater block (machined from one end of a 99.99 percent pure solid copper cylinder) placed on a steel base plate and forms the base of a cubic viewing chamber (15 cm each side). The test heater block was machined to a diameter of 88.9 mm and a height of 42.18 mm. Holes were drilled into the copper cylinder from bottom to insert several cartridge heaters. Temperature was measured with thermocouples embedded in the test block. The test liquid was confined to the viewing chamber and was boiled on the copper surface. A cooling coil made of copper tubing was placed just under the free surface of the test liquid. Antifreeze mixture (mixture of ethylene glycol and water) was used as a cooling fluid. The antifreeze mixture was chilled in an external chiller unit to $-15°C$ and pumped through the cooling coil to cool the test liquid and obtain the required degree of subcooling. The temperature drop of the cooling fluid in the chiller tubes was maintained at less than 1°C to ensure uniform cooling at the free surface. Complete details of the apparatus are given by Banerjee [11].

Visualization studies were performed to determine the interface motion. The viewing chamber was illuminated from outside with tungsten filament incandescent light source placed behind optical diffuser plates. Vapor bubbles were photographed with a digital camera (manufactured by HiSys Inc.) at framing rates ranging from 450 to 1024 frames/s. A measuring scale was glued on the side of the steel jacket for calibration of the digital video pictures. Simultaneous acquisition of thermocouple data for heat flux and wall temperature and video pictures for temporal variation of bubble height and bubble spacing was made. A few time exposure still photographs were also recorded on high speed photographic films. Various lense combinations ranging from 35–210 mm were tried for obtaining motion pictures on the video camera as well as for the still photographs. The pictures of the vapor bubbles on the heater were obtained by taking video pictures at an angle from the side of the viewing chamber. The angle of inclination, with respect to the horizontal plane, of the video camera varied from 5 deg to 20 deg. The distance between vapor bubbles was measured for vapor bubbles lying in a plane perpendicular to the viewing axis. This was done to obviate the optical distortions arising from the inclination of the camera.

Particle Tracking Velocimetry (PTV) Measurements. With the objective of studying the flow-field within the liquid pool at high subcoolings, the liquid pool above the heater was seeded with particles and the video pictures of the particle motion were recorded. Since a priori information was available about the optimum particle concentration, proper intensity and lighting techniques as well as the required camera parameters (e.g., magnification, resolution of the digital video camera, exposure time, etc.) for minimizing the errors in the data, the experimental procedure was based on trial and error. The particles used in this experiment were ground fish scales with a metallized coating of Aluminum. The particles had a nominal diameter of 10 μm. Also, the particles had widely varying density distribution—depending on the amount of metallized coating. Hence, particles with similar density as the test fluid (PF-5060) were obtained by floatation separation technique. In following this technique, particles were well stirred in a container of PF-5060. The particles with same density as liquid PF-5060 remained suspended in the liquid and were sucked out with a pipette, thus separating them from the floating particles at the free surface of the liquid and the particle sediments settled at the bottom of the container. This way a slurry of particles in PF-5060 was obtained with the solid particles having the same density as the liquid PF-5060.

The particles were introduced from above into the liquid pool during subcooled film boiling with a pipette and a plunger. The pipette was filled with the slurry of the particles in PF-5060 and was placed in the upper portion of the plane of imaging. The focal plane of the high speed digital camera was aligned with the illuminating plane. Illumination was achieved with a 600W Lowel Omni stage lamp (manufacturer: Omni Inc.) placed behind a collimator arrangement to generate a light sheet of approximately 1 mm thickness. He-Ne lasers of power rating 10mW, 100mW, and 300mW were also tried as illumination sources. However they were found to be unsuitable due to rapid attenuation of the illumination intensity of the light sheet.

To determine the flow field in the liquid, it was necessary to obtain simultaneous image of the particles and the vapor bubbles. Light scattered by the particles was sufficient to obtain an image on the digital video camera placed perpendicular to the light sheet. However, the light reflected by the vapor bubbles was insufficient to obtain an image on the digital video camera. Hence, a 60 W incandescent light source was placed on the side opposite to the camera, along with a set of diffuser plates to obtain a faint outline of the vapor bubbles in the images. This unconventional arrangement (compared to standard two-dimensional PTV) was necessi-

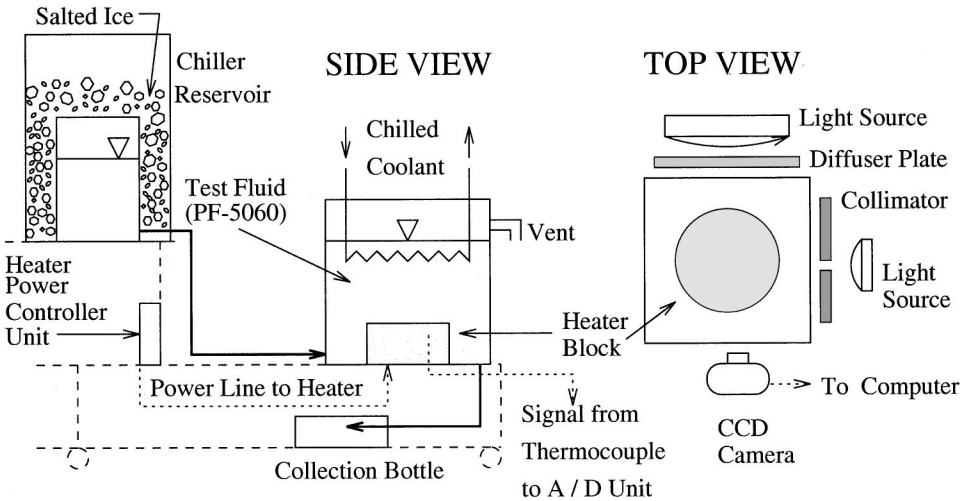

Fig. 1 Schematic diagram of experimental apparatus

tated by the need to obtain uniform background illumination as well as to restrict the illumination intensity to obtain images of particles and vapor bubbles at the same instant.

2.1 Experimental Procedure. The test surface was rubbed with 500 grit emery paper followed by 1000 grit emery paper and cleaned with acetone, prior to any test run. The test surface was heated to a temperature above the required superheat and the viewing chamber was filled with the test liquid to a certain fixed height.

A data acquisition system, consisting of a digital to analog converter and 16 channel data logger (manufacturer: Strawberry Tree), was used to record the signals from the thermocouples placed inside the copper block, on the outer surface of the steel jacket, in the test liquid, and the side walls of the test section.

The wall heat flux was adjusted by a variac to achieve the required superheat for obtaining film boiling under steady-state conditions. Tests were considered to be steady state when the temperature of the test block changed less than ± 1°C in 5 minutes. The liquid temperature changes were less than ± 0.5°C in 1 minute for liquid subcooling upto 20°C. Care was taken to avoid liquid thermal stratification. The liquid thermal stratification was found to be less than 0.5°C in a height of over 5 cm for subcoolings upto 20°C. The liquid subcooling was varied from 0 to 42°C and the wall superheat was varied from 50 to 100°C.

After steady state conditions were established the video camera was focussed on an area on the test surface for video capture of temporal evolution of vapor bubbles. The image of the measuring scale was recorded at the end of each experimental run for calibrating the magnification parameters of the camera and subsequent post processing for calculation of the bubble height.

2.2 Data Reduction

Wavelength Measurements. The radial location of bubbles was measured in pixels from the individual digital frames of the video pictures and converted to the actual distance, by multiplying with camera magnification. This enabled the measurement of the wavelengths in the radial direction. The circumferential direction wavelengths were obtained by counting the number of bubbles in each concentric ring. From this the average bubble separation distance in the circumferential direction was obtained by dividing the circumference of the ring by the number of bubbles.

Bubble Growth Rate Measurements. From the video films the height of the evolving interface was determined as a function of time. The interfacial velocity was obtained by taking the temporal derivative of the bubble height ($\zeta_{\max}$). The interfacial velocity in this situation is given by

$$\frac{d\zeta_{\max}}{dt} = \frac{(\Delta\zeta_{\max})}{(\Delta t)} \tag{1}$$

The growth rate is given by

$$\omega = \frac{\zeta_o}{\zeta_{\max}} \frac{d(\zeta_{\max}/\zeta_o)}{dt} = \frac{d}{dt}(\ln[\zeta_{\max}/\zeta_o]), \tag{2}$$

where, ζ_o is the undisturbed height of the vapor layer from the wall.

Particle Tracking Velocity Measurements. Using the ''pathline method,'' the velocity field in the liquid pool was measured with particles seeded in the liquid. In this method the displacement of a specific particle was measured between two consecutive video frames to obtain the velocity as

$$u = \frac{\Delta s}{S} f, \tag{3}$$

where s is the displacement of the particle, S is the magnification factor of the camera, and f is the framing rate of the video camera. The calculated value of the velocity was assigned to the mid-point between the initial and final locations of the particle.

Heat Flux Measurements. In steady-state tests, surface heat fluxes are readily calculated using the spatial temperature distribution recorded from the thermocouples. One-dimensional heat flow was found to exist inside the test heater block. The temperature distribution in the copper block was linear and the heat flux, q_W, was evaluated from the gradient of the temperature profiles in the copper block, as

$$q_W = \kappa_s \frac{\Delta T}{\Delta y}, \tag{4}$$

where κ_s is the thermal conductivity of heater test block material (copper), ΔT is the temperature differential between two thermocouples lying in the same vertical plane, and Δy is the distance between them. The surface temperature was obtained by simply extrapolating the temperature profile to the surface. Hence, the average wall Nusselt number $\overline{\overline{\mathrm{Nu}}}_W$ and the average heat transfer coefficient in film boiling $\bar{h}$ can be defined as

$$\overline{\overline{\mathrm{Nu}}}_W = \frac{q_W l_o}{\Delta T_W \kappa_v}; \quad \bar{h} = \frac{q_W}{\Delta T_W}. \tag{5}$$

The characteristic length scale, l_o and growth frequency, ω_o, in film boiling are defined as

$$l_o = \left[\frac{\gamma}{(\rho_l - \rho_v)g}\right]^{1/2}; \quad \omega_o = \left[\left(\frac{\rho_l - \rho_v}{\rho_l + \rho_v}\right)\left(\frac{g}{l_o}\right)\right]^{1/2}. \tag{6}$$

2.3 Error Analysis. The uncertainty in heat flux data is estimated to be ± 12 percent whereas the uncertainty in heat transfer coefficient values is estimated to be ± 15 percent. The error in measurement of interface height is estimated to be ± 10 percent, in interface velocity, ± 11 percent and in interface growth frequency ± 16 percent. For details of error analyses the reader is referred to Banerjee [11].

The net error in displacement measurement of particles in the PTV experiments is calculated to be ± 10 percent neglecting the three-dimensional effects of the velocity field. By including the three-dimensional effects in the velocity field this error is estimated to be less than 15 percent. The net error in velocity determination is estimated to be about ± 10.5 percent when neglecting the three-dimensional effects and is estimated to be about ± 15 percent when including the three-dimensional effects.

3 Results and Discussion

Experimental observations of interfacial behavior and wall heat transfer were made for a range of liquid subcoolings. At low liquid subcoolings the interface was observed to evolve as for saturated film boiling and vapor bubbles were released in a regular and cyclic manner from the interface. However, at high subcoolings the interface acquired a static shape. As such, discussion of results is divided into low and high subcooling cases.

3.1 Low Subcooling. For film boiling under subcooled conditions data were taken for dominant wavelength, interface shape, growth of interface, growth rate and for the heat transfer coefficient and comparisons were made with predictions.

Dominant Wavelength. Because of the passage through the pool of the bubbles leaving the interface, it was difficult to capture an unambiguous view of the orientation and location of the bubble releasing nodes at low subcoolings. However, with increased subcooling the interface acquired a nearly static shape, as will be discussed in more detail later. In this situation a clear view of the location of the bubble releasing nodes could be obtained. This is depicted in the photograph in Fig. 2. In this photograph the location of wave peaks in several radial rings and in the azimuthal direction can be clearly seen. It is in this context that Fig. 2 is contained in this section on low subcooling. From such photo-

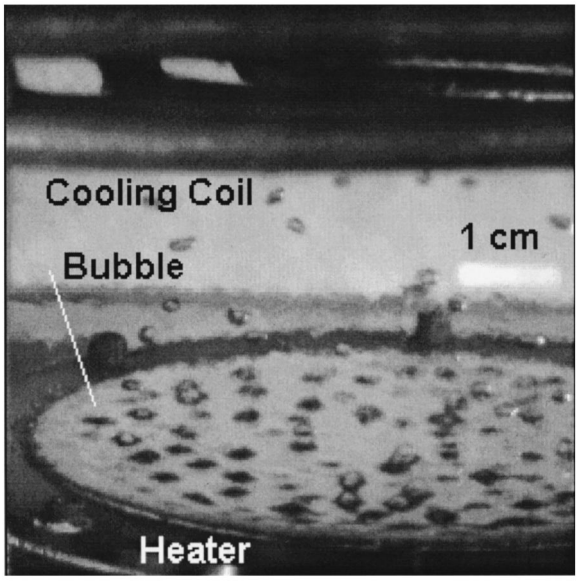

Fig. 2 Digital image of non-departing bubbles arranged on concentric rings on a horizontal circular plate for superheat of 52°C and subcooling of 42°C obtained from a single frame of movie. Camera angle: 10 deg to the horizontal. Test-Fluid: PF-5060. About 5 percent of the bubbles were found to depart by merger of contiguous bubbles caused by natural convection circulation induced into the liquid pool from the side walls.

graphs the ring radius as a function of discrete values of the ring number, n, from the center and the number of wave modes (m) in the n^{th} ring could be obtained. Figure 3 compares with the data the dimensionless value of ring radius as a function of ring number, n, with that predicted from the analysis. It is seen that though there is some variability in the data obtained from different experiments, the predictions are in general agreement with data. A similar comparison of the number of wave modes, m, as function of n is performed in Fig. 4. Although the agreement between predictions from analysis and data is reasonable, the data also show scatter. Some scatter in the data is not unexpected because of some lateral merger of bubbles. Any merger can reduce the number of wave modes by one, until the original pattern re-establishes. Good agreement with analytical predictions of the measured values of r_{n_d}, and m suggest that as assumed in the analysis the dominant

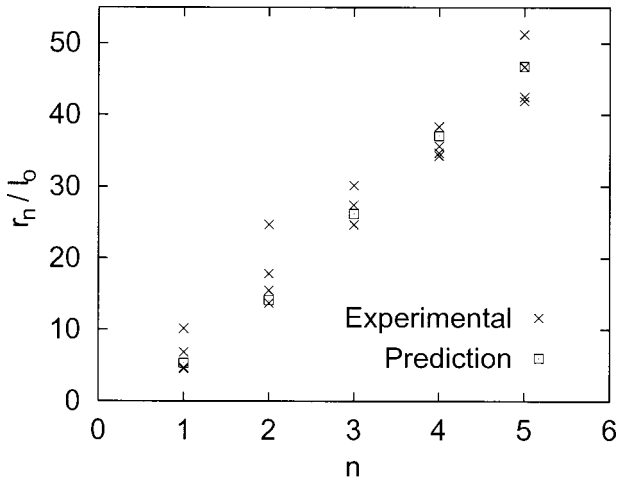

Fig. 3 Comparison of prediction for most probable values of r_n for different rings with the experimental measurements

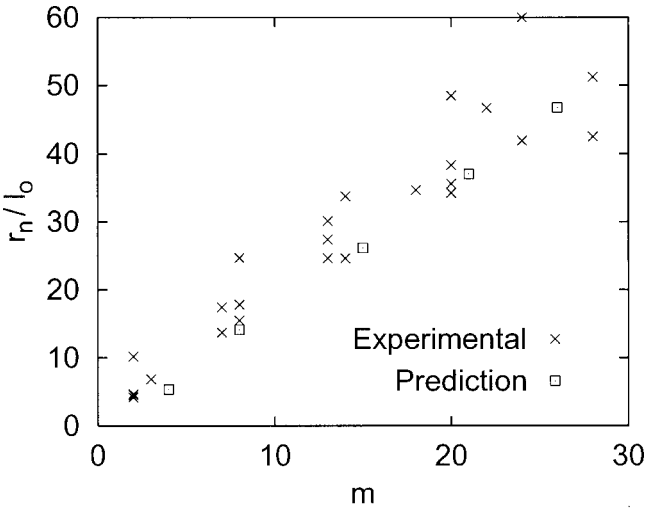

Fig. 4 Comparison of prediction for most probable values of r_n with the experimental measurements of number of crests in a ring

wavelength in the radial and azimuthal directions are the same and are equal to two-dimensional Taylor wavelength, λ_{d2}. By dividing the total surface area of the disc with the number of wave-nodes, the area supported by one node is found to be approximately λ_{d2}^2. This is within ± 5 percent of the predicted values.

Comparison of Interface Shapes. Comparison is made for the interface shape predictions from numerical simulations with vapor bubble pictures taken during experiments and is shown in Fig. 5, for subcooled film boiling of PF-5060 at a wall superheat of $\Delta T_W = 100°C$ and $\Delta T_{sub} = 10°C$. Three frames prior to bubble departure are shown in Fig. 5 in three separate rows. The picture

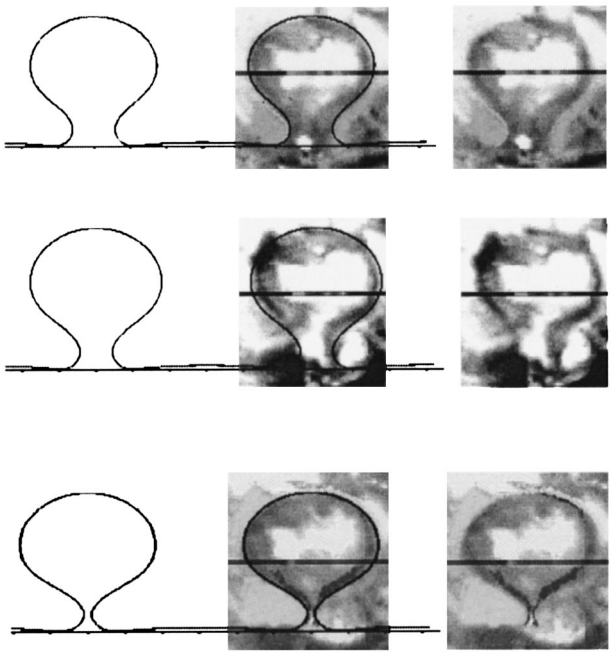

Fig. 5 Comparison of shapes of vapor bubbles obtained from experiments with numerical predictions of interface shape for subcooled film boiling of PF-5060 at a wall superheat of $\Delta T_W = 100°C$ and $\Delta T_{sub} = 10°C$. The pictures are at 1.2 ms intervals starting at 39.1 ms from the detected formation of the vapor bulge.

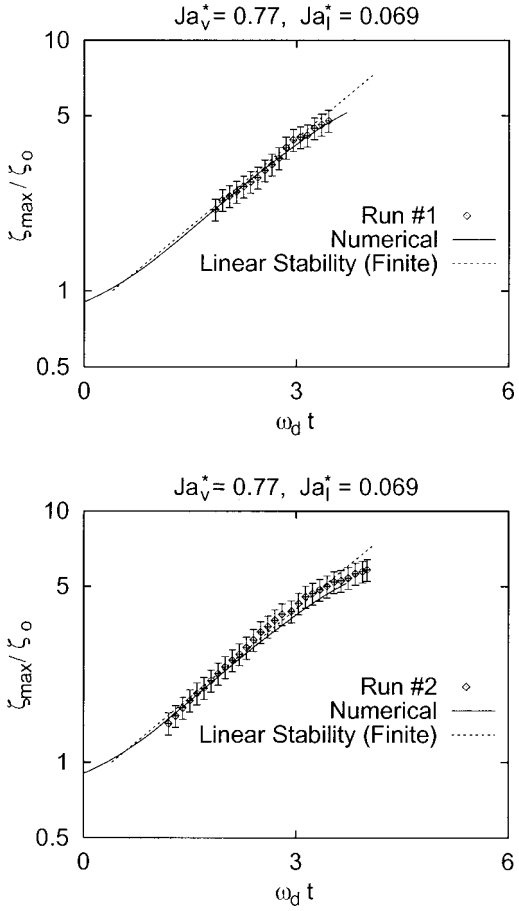

Fig. 6 Comparison of experimental data (denoted by various marker symbols) with numerical predictions (denoted by solid line) for temporal variation of bubble height for wall superheat, ΔT_W=100°C and liquid subcoolings, ΔT_{sub}=5°C. The dotted line represents prediction from linear stability theory.

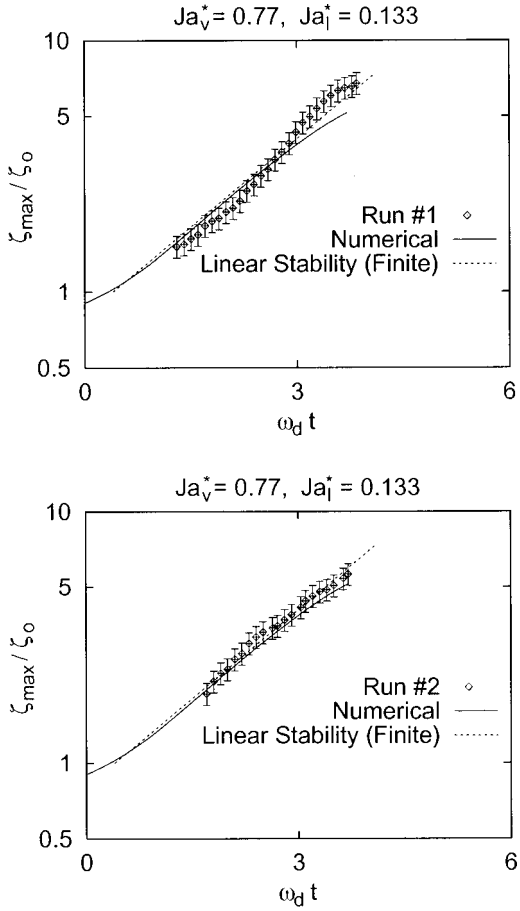

Fig. 7 Comparison of experimental data (denoted by various marker symbols) with numerical predictions (denoted by solid line) for temporal variation of bubble height for wall superheat, ΔT_W=100°C and liquid subcoolings, ΔT_{sub}=10°C. The dotted line represents prediction from linear stability theory.

on the right in each row was obtained from a single frame of the video motion picture recorded from experiments. The left plot in each row is the shape of the bubble obtained from numerical analyses at corresponding time step prior to bubble departure. In the middle of the predicted and observed bubble shapes is their superimposition. It is found that the predicted interfacial shapes agree quite well with the experimental data.

Interface Position. The highest position of the interface from the wall was measured in experiments and is plotted in Figs. 6 and 7 for liquid subcoolings of 5°C ($Ja_l^*=0.069$) and 10°C ($Ja_l^*=0.133$), respectively. In both cases data are plotted as a function of time from two different experiments. The interface height is normalized with initial vapor thickness of 0.77 mm and time is normalized with respect to inverse of the growth rate obtained from linear stability analysis for infinite fluid layers. In these figures the solid line represents prediction from the numerical simulations whereas the dotted line is from the linear stability theory. The last point on the solid lines represent the initial height just before departure and at the end of the measured growth period. The numerical simulations correctly predict the nonlinear behavior of the interface during its evolution, especially slowing down of the interface in the later stages of the end of growth period. The model generally tends to underpredict the maximum interface position just prior to bubble pinch off by about 10 percent. However the observed growth periods lie within ±10 percent of the predictions.

Growth Rate. The interface growth rate was obtained from data such as plotted in Figs. 6 and 7 by dividing the displacement at two consecutive times with the time interval between the two. The corresponding frequency normalized with the ''most dangerous frequency'' ($0.62\,\omega_o$) for infinite vapor-liquid layers is plotted in Figs. 8 and 9. In these figures the abscissa is the dimensionless position of the peak of the interface. The dotted line in these figures marks the ''most dangerous frequency'' (ω_{d_f}) where the vapor layer is assumed to have a finite thickness of 0.77 mm (ζ_o). The solid line is the prediction from the numerical simulations. The growth rate is predicted to increase to a maximum value as the interface evolves, acquire a nearly constant value before decreasing again to or below the finite vapor layer value before bubble ''pinch off.'' The predictions are seen to be in general agreement with the data, although the data show significant scatter. Two possible reasons for this large scatter are identified. One is the uncertainty (±16 percent) that exists when the derivative is obtained by taking a ratio of two small quantities. The second originates from the occasional merger of two neighboring bubbles. The merger resulted in the departure of a larger bubble. The wake left behind by the larger bubble distorted the flow field and caused an asymmetric growth rate of the interface in the vicinity.

Wall Heat Transfer. From the wall heat flux measured in steady state experiments and the deduced wall temperature, the heat transfer coefficient and in turn the area and time averaged

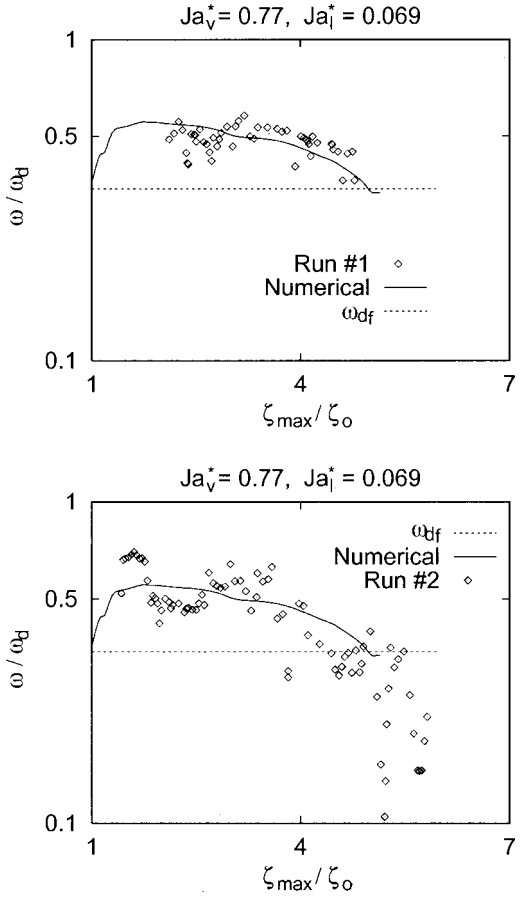

Fig. 8 Comparison of experimental data (denoted by various marker symbols) with numerical predictions (denoted by solid line) for temporal variation of bubble growth rate with bubble height. The dotted line represents prediction of growth rate, ω_{d_f}, from linear stability theory.

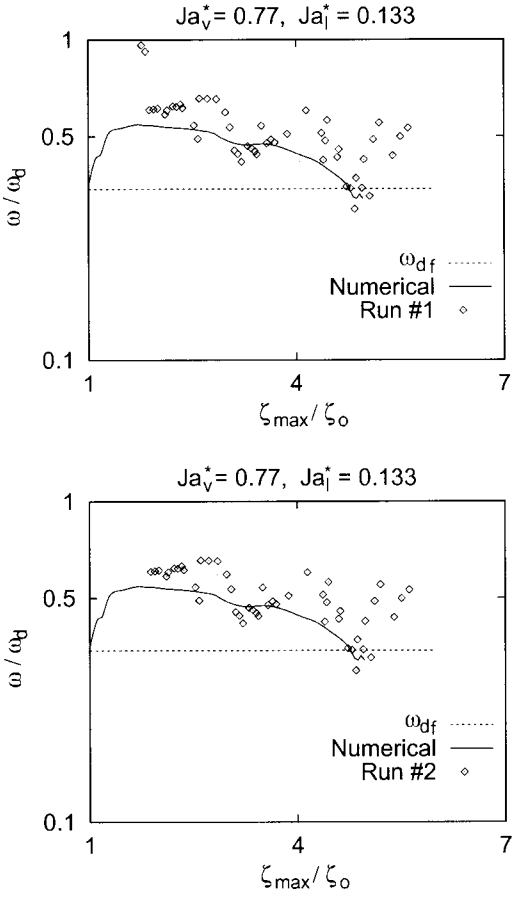

Fig. 9 Comparison of experimental data (denoted by various marker symbols) with numerical predictions (denoted by solid line) for temporal variation of bubble growth rate with bubble height. The dotted line represents prediction of growth rate, ω_{d_f}, from linear stability theory.

Nusselt number, $\overline{\overline{\mathrm{Nu}}}_W$ could be obtained. The values of $\overline{\overline{\mathrm{Nu}}}_W$ obtained in different experiments for liquid subcoolings upto 29.4°C are given in Table 1. In this table the values of $\overline{\overline{\mathrm{Nu}}}_W$ predicted from the numerical simulations are also listed. It should be noted that numerical predictions were made for constant heater surface temperature whereas the experiments were conducted by controlling the wall heat flux. It has been shown by Banerjee et al. [12] that because of spatial and temporal variations of the heat transfer coefficient, local heater surface temperature varies with time. However, for a thick copper surface the temperature variations are not expected to be significant and in turn the difference in the predicted heat transfer coefficient for constant wall temperature and for constant heat flux cases is expected to be quite small.

Figure 10 shows a comparison of the experimentally measured $\overline{\overline{\mathrm{Nu}}}_W$ with the numerical predictions as a function of liquid subcooling. It is found that the predictions are about 20 percent lower than the best fit through the data. Two possible reasons are advanced for this underprediction. One is the uncertainty that exists in the thermophysical properties of PF-5060 vapor, especially thermal conductivity and viscosity. The second is that the numerical simulations are based on a two-dimensional axisymmetric model of the film boiling process. In reality the process is three dimensional.

3.2 High Subcooling. At a wall superheat of 50°C and liquid subcooling greater than 38°C the interface was observed to acquire a near static shape. A photograph of the film boiling phenomena under static conditions of the interface is shown in Fig. 2. Under the static interface condition, however, about 3–5 percent of the vapor bubbles were observed to depart from the heater. Some bubble mergers occurred between the neighboring bubbles on the same ring as well as between bubbles lying on the adjacent rings. The radial as well as azimuthal movement of the bubbles is believed to result from the toroidal single phase convective cells that were present in the liquid. After bubble merger the orderly separation distance between the bubbles was distorted. However, subsequent to bubble departure, new bubble releasing nodes were seen to develop and the node separation distance was found to restore to its original value.

Flow Field. Particle Tracking Velocimetry (two-dimensional) provided the flow field in the liquid pool when the interface was nearly static. Figure 11 shows the liquid field obtained from particle velocimetry at intervals of 4 ms. Since particle density in pool was sparse (to facilitate localized measurements) particle positions from five consecutive video frames were combined together to obtain the information contained in each plot. The particle locations in each frame were mapped and the velocity field was evaluated from displacement of the particles. The viewing area was restricted to an area of 7 mm square in order to achieve the optimum resolution for the video camera. The viewing plane was chosen to begin just above the surface of the heater with the objective of studying the flow field above the interface. However, this placed a constraint on the measurements sincethe particle concentration tended to be lower near the wall due to lesser degree of convective motion just above the thin film region.

It is noted that velocity vectors in general show a downward motion in the region (valley) between two nodes. Above the crests (the larger bubble in Fig. 11) the velocity vectors are pointed

Table 1 Data obtained from low subcooling steady-state experiments.

ΔT_W	ΔT_{sub}	$\overline{\overline{Nu_W}}$	$\overline{\overline{Nu_W}}$
(°C)	(°C)	Exptl.	Numer.
98.6	0	9.7	
98.6	0	10.4	
102.3	0	9.7	7.94
102.3	0	9.9	
102.1	4.5	11.8	
102.1	4.5	11.5	
100	5	12.0	
102.2	6.2	11.1	
102.2	6.2	12.1	
101.4	7.9	10.7	
101.4	7.9	12.9	
100	10	12	8.45
99.1	11.2	10.1	
99.4	11.7	11.1	
102	14.6	11.1	
102	14.6	12.1	
99.1	21.5	11.1	8.91
99.1	21.5	12.1	
104.6	26.4	12.5	
104.6	26.4	12.0	
96.7	26.7	13.2	
98.9	29.4	14.2	
98.9	29.4	16.9	

upwards. The velocity vectors do show a general motion from right to left. It is believed that the cause of this motion is the toroidal convective cells that were also present in the liquid pool. Highest measured velocities of 100 mm/s are comparable to those predicted from the simulations of Banerjee et al. [10] for convection in a cylindrical cell with a bubble like protrusion at the bottom.

Heat Transfer. The Nusselt numbers based on the area and time averaged heat transfer coefficient obtained under the static mode are listed in Table 2. The data for the static mode was taken over a rather limited range of wall superheats and liquid subcoolings. In the static mode, vapor produced in the thin film region between adjacent bubbles is condensed at the upper surface of the bubble. As a result all of the energy transferred from the wall is dissipated into the pool through single phase natural convection. The vapor liquid interface and the surface of the cooling coils serve as high and low temperature surfaces, respectively. On the interface liquid suction (in the region where evaporation takes place) occurs. However, its effect on the natural convection heat transfer is considered to be small.

In the numerical simulation of the convective process in the circular cell surrounding a bubble, the height of the bubble protrusion was varied parametrically in the study by Banerjee et al. [10]. It was seen that the presence of the protrusion on the lower surface was to enhance the overall heat transfer. However, the effect was not significant, as in the range of parameters studied the enhancement was always less than 20 percent. Also the highest

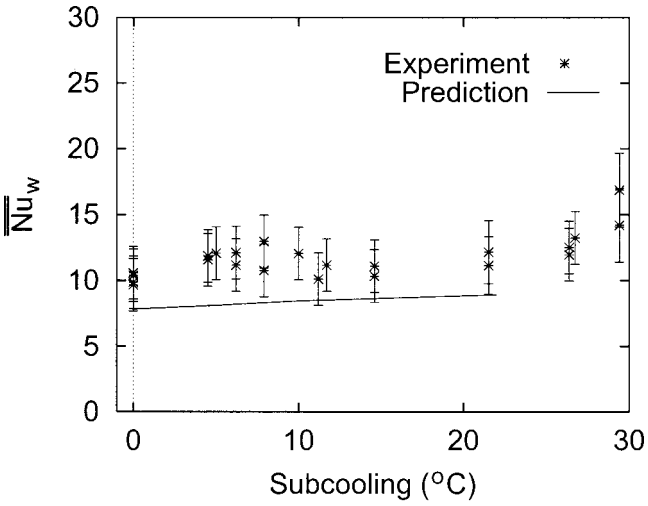

Fig. 10 Comparison of predictions for $\overline{\overline{Nu}}_W$ with experimental data for wall super-heat, $\Delta T_W = 100°C$, and liquid subcooling up to $\Delta T_{sub} = 22°C$

Rayleigh number considered in their work was 10^6. In Fig. 12, the Nusselt numbers predicted from their work are plotted as a function of Rayleigh number. The chainlines represent the extrapolation of their predictions to Rayleigh numbers upto 2×10^8. For the numerical analysis, Rayleigh number was based on the height H of the liquid layer above the interface (which was equal to 4 times the vapor bubble radius). For fluid properties of PF-5060 the value of H is 1.28 cm. In Fig. 12 the Nusselt numbers from Table 1 are also plotted. In plotting these data, the values listed in Table 2 were multiplied by $(\kappa_v/\kappa_l \times H/l_o)$. It is interesting to note that the results predicted from the extrapolated correlations nicely bound the data. Correlations for natural convection in cylinders with heated bottom, cooled top and insulated boundary have been reported by several investigators. Fishenden and Saunders [13] proposed a correlation of the form

$$\overline{\overline{Nu}} = 0.1 Ra^{1/3}, \tag{7}$$

whereas Chavanne et al. [14] proposed the correlation

$$\overline{\overline{Nu}} = 0.17 Ra^{2/7}. \tag{8}$$

In Fig. 12 these correlations are also plotted. It is noted that the observed value of Nusselt number is about 40 percent higher than the prediction from correlation of Fishenden and Saunders [13]. Some underprediction by correlation Eqs. 7 and 8 is expected since they were obtained for rigid bounding wall of the cylinder. In the present work near zero shear stress condition exists at the plane of symmetry between two nodes. Also, these correlations did not account for the presence of a protrusion at the lower surface.

4 Conclusions

1 Experimental validations of the numerical predictions for the evolution of the interface shape, temporal position of the interface, interface growth rates and wall heat flux values were performed. The numerical predictions are found to be in general agreement with the PF-5060 data obtained at low subcoolings.

2 The numerical simulations, generally underpredict the bubble height at departure by about 10 percent. However, the interface shape, interface evolution and interface growth rates prior to bubble departure are predicted within the range of experimental uncertainties. The growth rates of the liquid-vapor interface in subcooled film boiling were found to decrease with increase in subcooling.

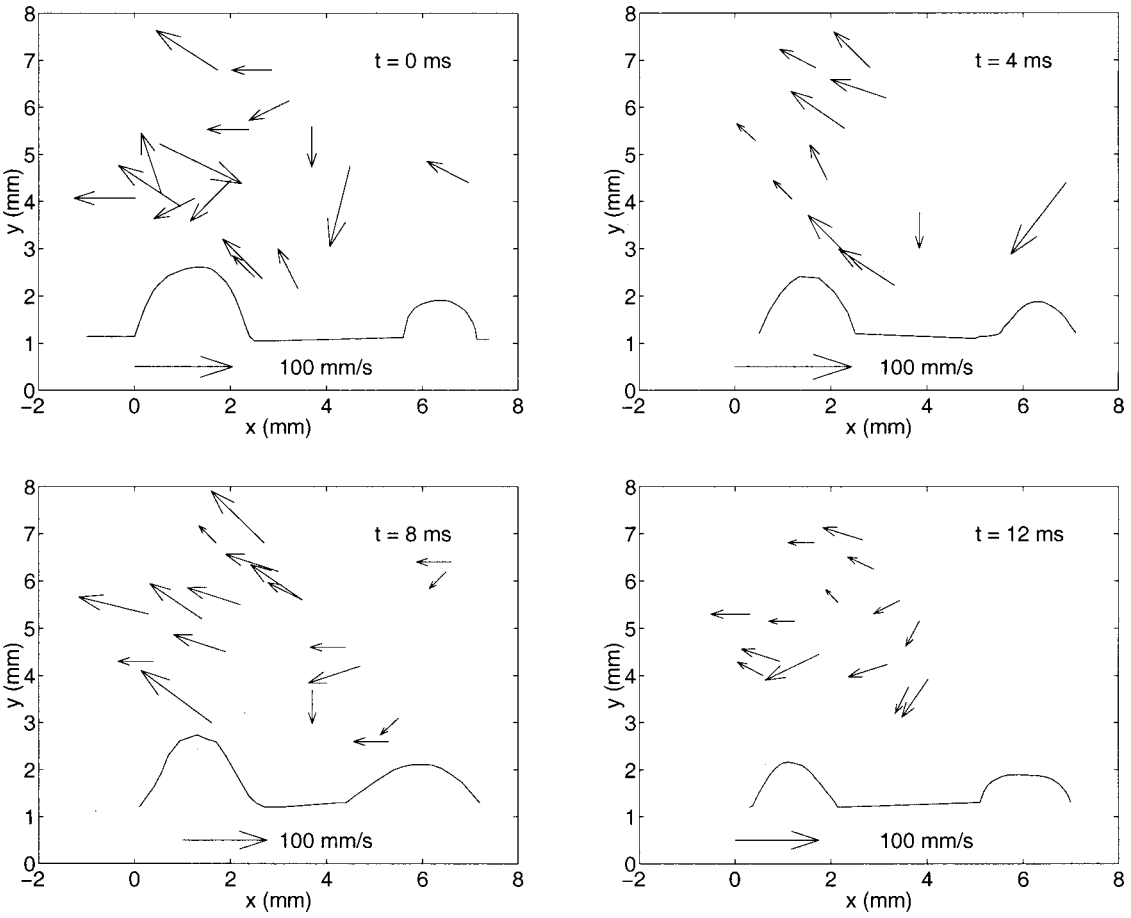

Fig. 11 Sample results from two-dimensional, PTV experiments showing the spatial distribution of velocity vectors at a particular instant. The frames are 4 ms apart. The protrusions depict outline of two vapor bubbles.

3 The wall heat flux values were underpredicted by about 20 percent for steady-state data. However, the model correctly predicts the rate of increase of wall heat transfer with increase in subcooling.

4 At high subcoolings the interface acquires a static shape.

5 The results from two-dimensional PTV experiments qualitatively match the velocity field predictions obtained from the static model of Banerjee et al. [10]. The flow in the liquid pool is towards the valleys and is away from the protrusions.

6 The experimental data for $\overline{\overline{Nu}}_W$ at high liquid subcoolings are bounded by the extrapolated results from the numerical model of Banerjee et al. [10] for the static bubble case. Correlations ob-

Table 2 Heat transfer results for high subcoolings

ΔT_W	ΔT_{sub}	$\overline{\overline{Nu}}_W$	q_W
(°C)	(°C)		$(W/m^2 \times 10^{-4})$
50.1	40	27.5	2.33
53.5	40	26.1	2.35
55	40	25.6	2.38
55	40	25.7	2.39
55	40	25.3	2.36
55.3	40	25.5	2.38
55.4	40	25.1	2.35
52.9	41	27.0	2.41
53.2	41	27.1	2.43
52.4	42	27.2	2.40
53.4	42	26.7	2.41
50.6	43	28.4	2.43
51.7	43	27.9	2.44
52	43	27.9	2.44
50.6	43	28.4	2.43
51.7	43	27.9	2.44
52	43	27.4	2.41

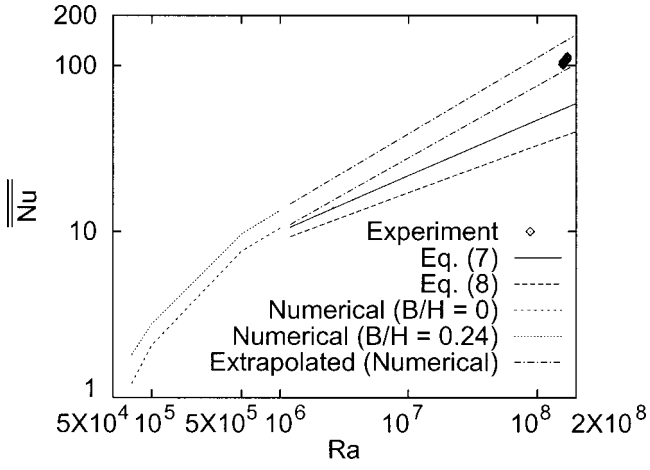

Fig. 12 Comparison of predictions for $\overline{\overline{Nu}}$ from numerical results of Banerjee et al. [10] for $B/H=0$ and $B/H=0.24$ with steady-state experimental data from Table 2. Correlction of Fishenden and Saunders [13] has been plotted as "Eq. (7)" and Correlation of Chavanne et al. [14] has been plotted as "Eq. (8)." Extrapolated trend lines for numerical predictions of Banerjee et al. [10] are also shown.

tained from literature for natural convection in circular cylinders underpredict the experimental values of $\overline{\overline{Nu}}_W$ by about 40 percent.

Nomenclature

B = height of bubble
f = camera framing rate
H = height of liquid pool above heater surface
m = wave number in the azimuthal direction
n = ring number in the radial direction
S = camera magnification factor
s = displacement
κ = thermal conductivity

Subscripts

max = maximum
d = corresponding to ''most dangerous'' or fastest growing wave
f = value obtained from linear stability theory
s = substrate heater property

Superscripts

$^{=}$ = space and time average quantity

References

[1] Dhir, V. K., and Purohit, G. P., 1978, ''Subcooled Film-Boiling Heat Transfer From Spheres,'' Nucl. Eng. Des., **47**, No. 1, pp. 49–66.
[2] Vijaykumar, R., and Dhir, V. K., 1992, ''An Experimental Study of Subcooled Film Boiling on a Vertical Surface-Hydrodynamic Aspects,'' ASME J. Heat Transfer, **114**, No. 1, pp. 161–168.
[3] Vijaykumar, R., and Dhir, V. K., 1992, ''An Experimental Study of Subcooled Film Boiling on a Vertical Surface-Thermal Aspects,'' ASME J. Heat Transfer, **114**, No. 1, pp. 169–178.
[4] Nishio, S., and Ohtake, H., 1992, ''Natural-Convection Film-Boiling Heat Transfer (Film Boiling from Horizontal Cylinders in Middle and Small-Diameter Regions),'' JSME Int. J., Ser. II, **35**, No. 4, pp. 380–388.
[5] Kikuchi, Y., Ebisu, T., and Michiyoshi, I., 1992, ''Measurement of Liquid-Solid Contact in Film Boiling,'' Int. J. Heat Mass Transf., **35**, No. 6, pp. 1589–1594.
[6] Busse, F. H., and Schubert, G., 1971, ''Convection in a Fluid with Two Phases,'' J. Fluid Mech., **46**, Part 4, pp. 801–812.
[7] Busse F. H., 1989, *The Fluid Mechanics of Astrophysics and Geophysics*, Vol. 4, W. R. Peltier, ed., Gordon and Breach, New York.
[8] Ahlers, G., Berge, L. I., Cannell, D. S., 1993, ''Thermal Convection in the Presence of a First-Order Phase Change,'' Phys. Rev. Lett., **70**, No. 16, pp. 2399–2402.
[9] Ayazi, F., and Dhir, V. K., 1987, ''A Thermal and Hydrodynamic Limit for Minimum Heat Flux and Wall Superheat During Subcooled Film Boiling on a Horizontal Cylinder,'' *AIAA 22nd Thermophysics Conference*, June 8–10, Honolulu, Hawaii, Paper No. AIAA-87-1535.
[10] Banerjee, D., Son, G., and Dhir, V. K., 1998, ''Natural Convection in a Cylindrical Section with a Static Protrusion: Numerical Simulation Relevant to Subcooled Film Boiling,'' *Proceedings of the 11th Intl. Heat Tr. Conf.*, **3**, August 23–28, 1998, Kyongju, Korea.
[11] Banerjee, D., 1999, ''Numerical and Experimental Investigation of Subcooled Film Boiling on a Horizontal Plate,'' Ph.D. thesis, University of California, Los Angeles; CA.
[12] Banerjee, D., Son, G., and Dhir, V. K., 1996, ''Conjugate Thermal and Hydrodynamic Analysis of Saturated Film Boiling From a Horizontal Surface,'' Proc. of the 1996 IMECE, Atlanta, GA, Nov. 17–22.
[13] Fishenden, M., and Saunders, O. A., 1950, ''An Introduction to Heat Transfer,'' Oxford University Press, London.
[14] Chavanne, X., Castaing, B., Chabaud, B., Chilla, F., and Hebral, B., 1998, ''Rayleigh Benard Convection at Very High Rayleigh Numbers Close to the ^{4}He Critical Point,'' Cryogenics, **38**, pp. 1191–1198.